Alexandria Engineering Journal (2015) 54, 981–992

HOSTED BY

Alexandria University

Alexandria Engineering Journal

www.elsevier.com/locate/aej
www.sciencedirect.com

ORIGINAL ARTICLE

Chaotic convection in a rotating fluid layer

Vinod K. Gupta [a,b,*], B.S. Bhadauria [a], I. Hasim [c], J. Jawdat [c], A.K. Singh [a]

[a] Department of Mathematics, Banaras Hindu University, Varanasi, India
[b] Department of Mathematics, DIT University, Dehradun, India
[c] Universiti of Kebansberg, Malaysia

Received 7 March 2015; revised 23 August 2015; accepted 1 September 2015
Available online 26 October 2015

KEYWORDS

Chaotic behavior;
Rotation;
Lorenz-equation;
Fluid layer

Abstract A study of thermal convection in a rotating fluid layer is investigated based on the dynamical systems approach. A system of differential equation like Lorenz model has been obtained by using Galerkin-truncated approximation. The chaotic convection is investigated in a rotating fluid layer. A low-dimensional, Lorenz-like model was obtained using Galerkin truncated approximation. The fourth-order Runge–Kutta method is employed to obtain the numerical solution of Lorenz-like system of equations. We found that there is proportional relation between Taylor number and the scaled Rayleigh number R. This means that chaotic behavior can be delayed (for increasing value of R) when we increase the scaled Taylor number. We conclude that the transition from steady convection to chaos depends on the level of Taylor number.

1. Introduction

Chaotic convection in fluid layer has great interest due to its relevance in a wide range of industrial applications. Chaos was obtained in a three dimensional phase space for the Lorenz [13] system arising from the truncation of the classical Rayleigh–Benard convection model. Chaotic behavior in a fluid layer can be actually advantageous in various industrial applications such as the production of crystals, oil reservoir modeling, and catalytic packed beds filtration.

The study of the effect of external rotation on thermal convection has attracted significant experimental and theoretical interest. Because of its general occurrence in geophysical and oceanic flows, it is important to understand how the Coriolis force influences the structure and transport properties of thermal convection. Rotating thermal convection also provides a system to study hydrodynamic instabilities, pattern formation and spatio-temporal chaos in nonlinear dynamical systems. The study of thermal convection in rotating fluid layer is motivated both theoretically and by its practical applications in engineering. Some of the important areas of applications in engineering include the food processing, chemical process, solidification and centrifugal casting of metals and rotating machinery. Bhadauria [6] investigated the fluid convection in a rotating porous layer under modulated temperature on the boundaries. They found that the effect of increasing the value of Taylor number is to delay the onset of convection, thus making the system more stabilizing. Similar results were found by Malashetty and Swamy [7] and Malashetty and Heera [8] for Taylor number.

* Corresponding author at: Department of Mathematics, Banaras Hindu University, Varanasi, India. Tel.: +91 9408686412.
E-mail addresses: vinodguptabhu@gmail.com (V.K. Gupta), mathsbsb@ yahoo.com (B.S. Bhadauria), ishak_h@ukm.my (I. Hasim), jadjawdat@gmail.com (J. Jawdat), ashok@bhu.ac.in (A.K. Singh).
Peer review under responsibility of Faculty of Engineering, Alexandria University.

http://dx.doi.org/10.1016/j.aej.2015.09.002

Nomenclature

Latin symbols

a	horizontal wave number
a_c	critical wave number
$\mathbf{g}$	gravitational acceleration, $(0,0,-g)$
d	height of fluid layer
p	pressure
Pr	Prandtl number, ν/κ_T
T_a	Taylor number, $\frac{4d^4\Omega^2}{\nu^2}$
$\mathbf{q}$	velocity of the fluid (u,v,w)
Ra	Rayleigh number, $\alpha_T g d(\Delta T)d^3/\nu\kappa_T$
t	time
T	temperature
ΔT	temperature difference between the walls

Greek symbols

Ω	angular velocity, $(0,0,\omega)$
κ_T	thermal diffusivity
α_T	thermal expansion coefficient
ρ	density
ν	kinematic viscosity, μ/ρ_0
ψ	stream function

Subscripts

b	basic state
c	critical
0	reference state
cr	critical value

Superscripts

$'$	perturbed value
$*$	non-dimensional value

There are several computational results on the effect of rotation in porous media. Vadasz and Olek [11] found that the transition from steady convection to chaos occurs by a subcritical Hopf bifurcation producing a solitary cycle which may be associated with a homoclinic explosion when the Prandtl number is low. The work of Vadasz [15] suggests an explanation for the appearance of this solitary limit cycle via local analytical results. Mahmud and Hasim [1] investigated effect of magnetic field on chaotic convection in fluid layer. He observed that transition from chaotic convection to steady convection occurs by a subcritical Hopf bifurcation producing a homoclinic explosion which may be limit cycle as Hartman number increases. Jawdat and Hasim [2] found that the onset of chaotic convection in a porous medium for a low Prandtl number, amount of internal heat generation is inversely proportional to scaled Rayleigh number. The generalized Lorenz models and their routes to chaos by energy-conserving horizontal mode truncations were investigated by Roy and Musielek [9]. They observe that $5D$ system is the lowest-order generalized Lorenz model, which can be constructed by horizontal modes. Vadasz and Olek [17] observed that when the Prandtl number is moderate, the route to chaos occurs by a period doubling sequence of bifurcations. The work of Vadasz [16] suggests an explanation for the appearance of this solitary limit cycle via local analytical results.

Mahmud and Hasim [18] investigated chaotic convection in porous media in the presence of feedback control. They observed chaotic behavior with increasing Rayleigh number. Magyari [10] demonstrated that the structure of the feedback control system proposed by Mahmud and Hasim [18] does not change the original uncontrolled system but its effect is in altering the initial conditions of the system. Sheu [4] demonstrated that interface heat transfer the route to chaos and that application of a thermal non-equilibrium model tends to stabilize steady convection. Sheu et al. [5] investigated that stress relaxation tends to accelerate the onset of chaos through the use of an oldroydian fluid. Ferrario et al. [3] studied the chaotic behavior of second grade fluid in two dimensional convection. Gupta and Singh [19] reported the effect of anisotropic parameters on chaotic convection. They found a proportional relation between scaled Rayleigh number and scaled anisotropic parameters. Gupta and Bhadauria [20] investigated the double diffusive convection in a couple stress liquid saturated porous layer with Soret effect using thermal non-equilibrium model. Gupta et al. [21] studied the effect of applied magnetic field in couple stress fluid. They found that increase in Hartmann number increases the level of chaos. Also, Gupta and Singh [22] investigated the effect of chemical reaction in double diffusive convection.

In this study, the work of Vadasz [12] on the transition to chaos in rotating porous layer is extended to include consideration of rotating fluid layer. The transition from steady convection to chaos was analyzed by using Runge–Kutta method of order four. The Galerkin truncated approximation was applied to the governing equations for thermal convection in a rotating fluid layer subject to gravity and heated from below, allowing us to deduce an autonomous system with four ordinary differential equations. This system is investigated for the dynamic behavior of thermal convection in a fluid layer and for the effect of rotation on transition to chaos.

2. Mathematical formulation

We consider a horizontal rotating fluid layer of depth d between two parallel infinite stress free boundaries, which is heated from below and cooled from above. The x-axis is taken along the lower boundary, and the z-axis vertically upward. The lower surface is held at temperature T_0, while the upper surface is at $T_0+\Delta T$, where ΔT is temperature difference between the lower and upper surfaces. The continuity and momentum equations governing the motion of an incompressible rotating fluid are given by

$$\nabla\cdot\vec{q}=0 \tag{1}$$

$$\frac{\partial\vec{q}}{\partial t}+2\Omega\times\vec{q}=-\frac{1}{\rho_0}\nabla p+\frac{\rho}{\rho_0}\vec{g}+\nu\nabla^2\vec{q} \tag{2}$$

Table 1 Values of R where λ_2, λ_3 become equal and complex conjugates.

T	R
0.0	24.73684209
0.05	25.07354964
0.1	25.55198983
0.15	26.14758062
0.2	26.84255860
0.215	27.06837743
0.25	27.62381051
0.45	31.44507647
0.6	34.90344691

$$\frac{\partial T}{\partial t} + (\vec{q}\cdot\nabla)T = \kappa_T \nabla^2 T \tag{3}$$

$$\rho = \rho_0[1 - \alpha_T(T - T_0)] \tag{4}$$

The thermal boundary condition is

$$T = T_0 + \Delta T \quad \text{at } z = 0 \quad \text{and} \quad T = T_0 \quad \text{at } z = d \tag{5}$$

where $\vec{q}$ is velocity of fluid, Ω the vorticity vector, p the fluid pressure, ρ the density of fluid, v the kinematic viscosity, κ_T the thermal diffusivity ratio, and α_T the thermal expansion coefficient of fluid.

2.1. Basic state

The basic state of the fluid is quiescent and is given by,

$$\mathbf{q}_b = (0,0,0), \qquad p = p_b(z), \qquad T = T_b(z) \tag{6}$$

Using Eq. (6) in Eqs. (1)–(3) we get,

$$\frac{dp_b}{dz} = \rho_b \vec{g}, \quad \frac{d^2 T_b}{d^2 z} = 0, \quad \rho_b = \rho_0[1 - \alpha_T(T_b - T_0)] \tag{7}$$

2.2. Perturbed state

On the basic state we superpose perturbations in the form

$$\vec{q} = \vec{q}_b + \vec{q}', \quad T = T_b(z) + T', \quad p = p_b(z) + p',$$
$$\rho = \rho_b(z) + \rho' \tag{8}$$

where primes indicate perturbations. Substituting Eq. (8) into Eqs. (1)–(4) and using the basic state solutions, we obtain the equations governing the perturbations in the form,

$$\nabla\cdot\vec{q}' = 0 \tag{9}$$

$$\frac{\partial \vec{q}'}{\partial t} + 2\Omega\times\vec{q}' = -\frac{1}{\rho_0}\nabla p' + \frac{\rho'}{\rho_0}\vec{g} + v\nabla^2\vec{q}' \tag{10}$$

$$\frac{\partial T'}{\partial t} + (\vec{q}'\cdot\nabla)T' + w'\frac{\partial T_b}{\partial z} = \kappa_T\nabla^2 T' \tag{11}$$

we consider only two-dimensional disturbances and define stream function ψ and $\vec{g}$ by

$$(u', w') = \left(-\frac{\partial\psi}{\partial z}, \frac{\partial\psi}{\partial x}\right), \qquad \vec{g} = (0,0,-g) \tag{12}$$

which satisfy continuity Eq. (9).

Eliminating pressure term from Eq. (10), introducing the stream function ψ and non-dimensionalizing the resulting equation as well as Eqs. (10) and (11) use the following non-dimensional parameters: $(x', y', z') = d(x^*, y^*, z^*)$, $t' = \frac{d^2}{\kappa_T}t^*, T' = (\Delta T)T^*, p' = \frac{\mu\kappa_T}{d^2}p^*$ to obtain non-dimensional equations

$$\left[\left(\frac{1}{Pr}\frac{\partial}{\partial t} - \nabla^2\right)^2\nabla^2 + T_a\frac{\partial^2}{\partial z^2}\right]\frac{\partial\psi}{\partial x} = Ra\frac{\partial^2}{\partial x^2}\left(\frac{1}{Pr}\frac{\partial}{\partial t} - \nabla^2\right)T \tag{13}$$

$$\left(\frac{\partial}{\partial t} - \nabla^2\right)T = \frac{\partial\psi}{\partial x} - \frac{\partial(\psi, T)}{\partial(x, z)} \tag{14}$$

where $Pr = \frac{v}{\kappa_T}$, Prandtl number, $T_a = \frac{4d^4\Omega^2}{v^2}$, Taylor number, $Ra = \frac{\alpha(\Delta T)d^3 g}{v\kappa_T}$, Rayleigh number.

Assumed, boundaries are stress free and isothermal; therefore, the boundary conditions are given by

$$w = \frac{\partial^2 w}{\partial z^2} = T = 0 \quad \text{at } z = 0 \quad \text{and } z = 1 \tag{15}$$

The set of partial differential Eqs. (13) and (14) forms a non-linear coupled system with the boundary conditions. We will solve this by using Galerkin method.

3. Truncated Galerkin expansion

To obtain the solution of non-linear coupled system of partial differential Eqs. (13) and (14), we represent the stream function and temperature in the form

$$\psi = A_1\sin(ax)\sin(\pi z) \tag{16}$$

$$T = B_1\cos(ax)\sin(\pi z) + B_2\sin(2\pi z) \tag{17}$$

This representation is equivalent to Galerkin expansion of the solution in both the x- and z-directions. Substituting Eqs. (16) and (17) in Eqs. (13) and (14), multiplying the equations by the orthogonal characteristic functions corresponding to Eqs. (16) and (17) and integrating them over the domain $[0,1]\times[0,1]$ yield a set of three ordinary differential equations for the time evolution of the amplitudes:

$$\frac{d^2A_1(\tau)}{d\tau^2} = -2Pr\frac{dA_1(\tau)}{d\tau} + \frac{A}{k^6}(a^2Ra - \pi^2T_aPr - k^6Pr)A(\tau) + \frac{\pi a^2 PrRa}{k^6}A(\tau)B_2(\tau) + \frac{aRaPr(Pr-1)}{k^4}B_1(\tau) \tag{18}$$

$$\frac{dB_1(\tau)}{d\tau} = \frac{a}{k^2}A(\tau) + \frac{\pi a}{k^2}A_1(\tau)B_2(\tau) - B_1(\tau) \tag{19}$$

$$\frac{dB_2(\tau)}{d\tau} = -\frac{4\pi^2}{k^2}B_2(\tau) - \frac{\pi a}{2k^2}A_1(\tau)B_1(\tau) \tag{20}$$

where $k^2 = \pi^2 + a^2$, total wavelength number and time is rescaled by $\tau = k^2 t$.

Although we cannot establish the relationship between the solutions of the governing partial differential and the

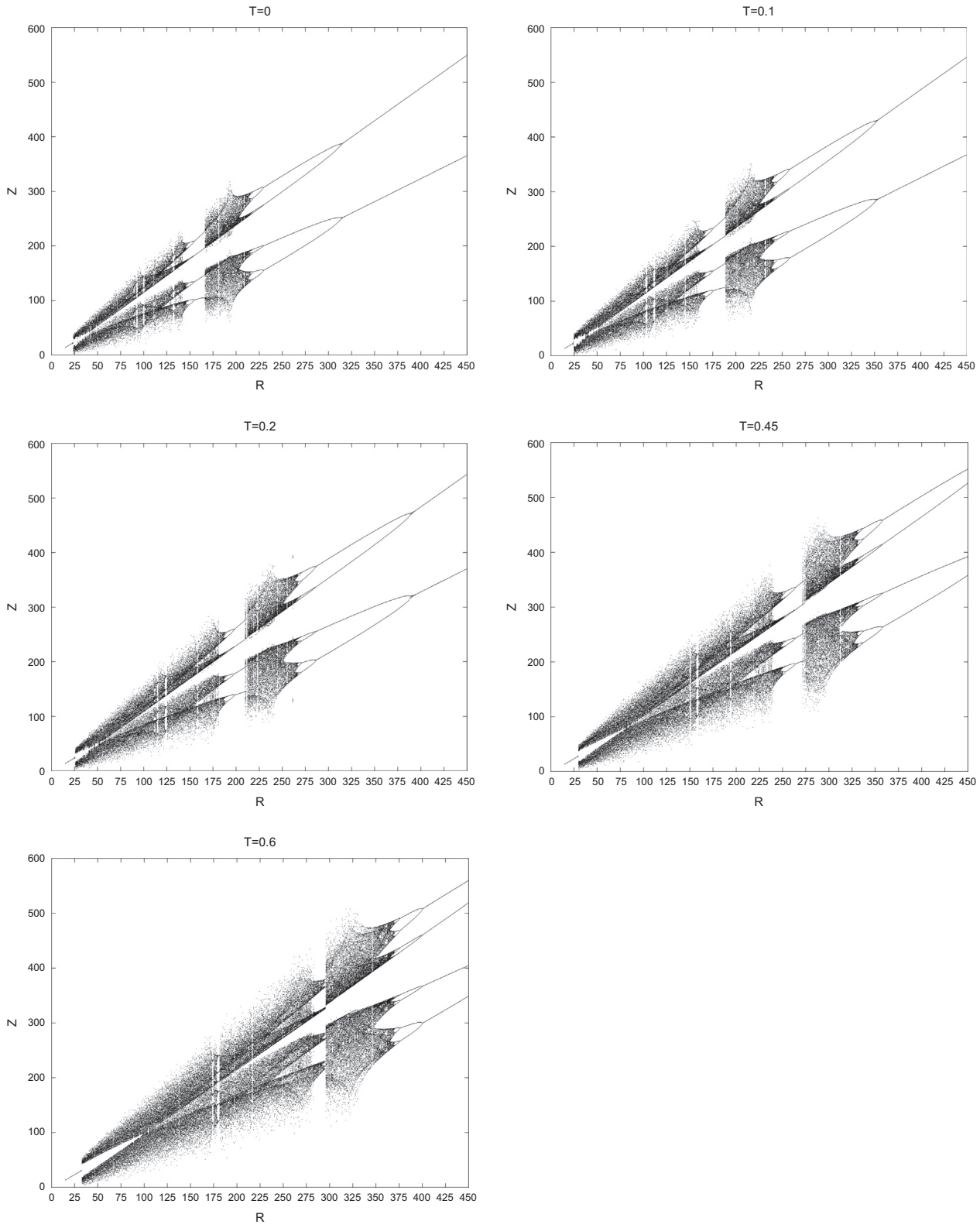

Fig. 1 Bifurcation diagrams of Z versus R representing maxima and minima of the post-transient solution of $Z(t)$ for $\sigma = 10, \gamma = -8/3$.

corresponding truncated ordinary differential system, these lower-order spectral models may qualitatively reproduce the convective phenomena observed in the full system. The result can also be used as starting values when discussing the fully non-linear problem.

It is convenient to introduce the following notation:

$$R = \frac{a^2 Ra}{k^6}, \quad T = \frac{\pi^2 T_a}{k^6} \quad \text{and} \quad \gamma = -\frac{4\pi^2}{k^2}, \quad \sigma = Pr \tag{21}$$

and rescale the amplitudes in the form of

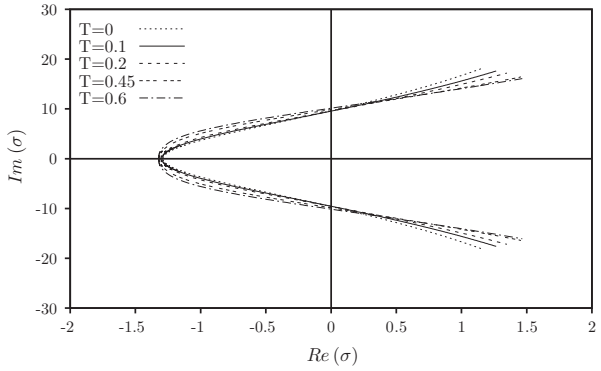

Fig. 2 Evolution of complex eigenvalues with increasing Rayleigh number, for $T = 0, 0.1, 0.2, 0.45, 0.6$.

$$X(\tau) = \frac{\pi a}{k^2\sqrt{2}} A_1(\tau), \quad Y(\tau) = \frac{\pi R}{\sqrt{2}} B_1(\tau) \quad \text{and}$$
$$Z(\tau) = -\pi R B_2(\tau) \tag{22}$$

to provide the following set of equations:

$$\dot{X} = W \tag{23}$$

$$\dot{Y} = RX - XZ - Y \tag{24}$$

$$\dot{Z} = XY + \gamma Z \tag{25}$$

$$\dot{W} = -2\sigma W + \sigma\{R - \sigma(T+1)\}X - \sigma XZ + \sigma(\sigma - 1)Y \tag{26}$$

where the dots$(\cdot)$ denote the time derivative $d()/d\tau$. Eqs. (23)–(26) are like the Lorenz equations (Lorenz [13], Sparrow [14]), although the different coefficients.

4. Stability analyses

In this section, we consider the thermal instability of buoyancy-driven flow of a rotating fluid layer confined between stress-free boundaries. The fluid layer is subjected to a constant horizontal temperature gradient. Stability analysis of the stationary solutions was performed in order to determine the nature of dynamics about the fixed points. The non-linear dynamics of Lorenz-like system (23)–(26) has been analyzed and solved for $\sigma = 10$ and $\gamma = -8/3$ corresponding to convection. The basic properties of the system to obtain the eigenfunction are described next.

4.1. Dissipation

System (23)–(26) is dissipative since

$$\nabla V = \frac{\partial \dot{X}}{\partial X} + \frac{\partial \dot{Y}}{\partial Y} + \frac{\partial \dot{Z}}{\partial Z} + \frac{\partial \dot{W}}{\partial W} = -(2\sigma + 1 - \gamma) < 0 \tag{27}$$

Hence, if set of initial points in the phase space occupies region $V(0)$ at time $t = 0$, then after some time t, the endpoints of the trajectories will decrease a volume

$$V(t) = V(0)\exp\left[-(2\sigma + 1 - \gamma)t\right] \tag{28}$$

The above expression shows that the volume decreases exponentially with time.

4.2. Equilibrium points

System (23)–(26) has the general form $\dot{X} = f(X)$ and the equilibrium (fixed or stationary) points X_s are defined by $f(X_s) = 0$. The equilibrium points of the rescaled system are

$$(X_1, Y_1, Z_1) = (0, 0, 0) \tag{29}$$

and

$$\left.\begin{aligned} X_{2,3} &= \pm\sqrt{\tfrac{\gamma(T+1-R)}{T+1}} \\ Y_{2,3} &= \pm\sqrt{\gamma(T+1-R)(T+1)} \\ Z_{2,3} &= -(T+1-R) \end{aligned}\right\} \tag{30}$$

corresponding to the motionless and convection solutions.

4.3. Stability of equilibrium points

By linearizing system (23)–(26), we obtain its Jacobian matrix as follows:

$$J = \begin{bmatrix} 0 & 0 & 0 & 1 \\ R - Z & -1 & -X & 0 \\ Y & X & \gamma & 0 \\ \sigma\{R - \sigma(T+1) - Z\} & \sigma(\sigma - 1) & -\sigma X & -2\sigma \end{bmatrix} \tag{31}$$

The characteristic values of the Jacobian matrix, obtained by solving the zeros of the characteristic polynomial, provide the stability conditions. A fixed point is stable if all the eigenvalues are negative (or in the case of complex eigenvalues, they have negative real parts) and unstable, when at least one eigenvalue becomes positive (or in the case of complex eigenvalues, it has positive real part).

The stability of the fixed point corresponding to motionless solution $X_1 = 0, Y_1 = 0, Z_1 = 0$ is controlled by the zeros of the following characteristic polynomial equation for the eigenvalues, $\lambda_i (i = 1, 2, 3, 4)$:

$$(\lambda - \gamma)\left[\lambda^3 + (2\sigma + 1)\lambda^2 + \{\sigma^2(T+1) + (2 - R)\sigma\}\lambda + \sigma^2(T + 1 - R)\right] = 0 \tag{32}$$

The first eigenvalue $\lambda_1 = \gamma$ is always negative as $\gamma = -8/3$, but the other three eigenvalues are given by equation

$$\lambda^3 + (2\sigma + 1)\lambda^2 + \{\sigma^2(T+1) + (2 - R)\sigma\}\lambda + \sigma^2(T + 1 - R) = 0 \tag{33}$$

which provides the stability condition for the motionless solution in the form $R < T + 1$. Therefore the critical value of R, where the motionless solution loses stability and the convection solution (expressed by the other two fixed points) takes over, is determined as

$$R_{c1} = R_{cr} = 1 + T \tag{34}$$

which corresponds to $Ra_{cr} = k^6(1 + T)/a^2$.

The stability of the fixed points corresponding to the convection solution $(X_{2,3}, Y_{2,3}, Z_{2,3})$ is controlled by the following equation for the eigenvalues, $\lambda_i (i = 1, 2, 3, 4)$:

$$\lambda^4 + (2\sigma + 1 - \gamma)\lambda^3 + \left[\frac{-\gamma R}{T+1} + 2\sigma(1 - \gamma) + \sigma(\sigma - 1)(T+1)\right]\lambda^2 + \left[\frac{-2\sigma\gamma R}{T+1} + \sigma\gamma\{(2 - \sigma)(T+1) - R\}\right]\lambda + 2\sigma^2\gamma(T + 1 - R) = 0 \tag{35}$$

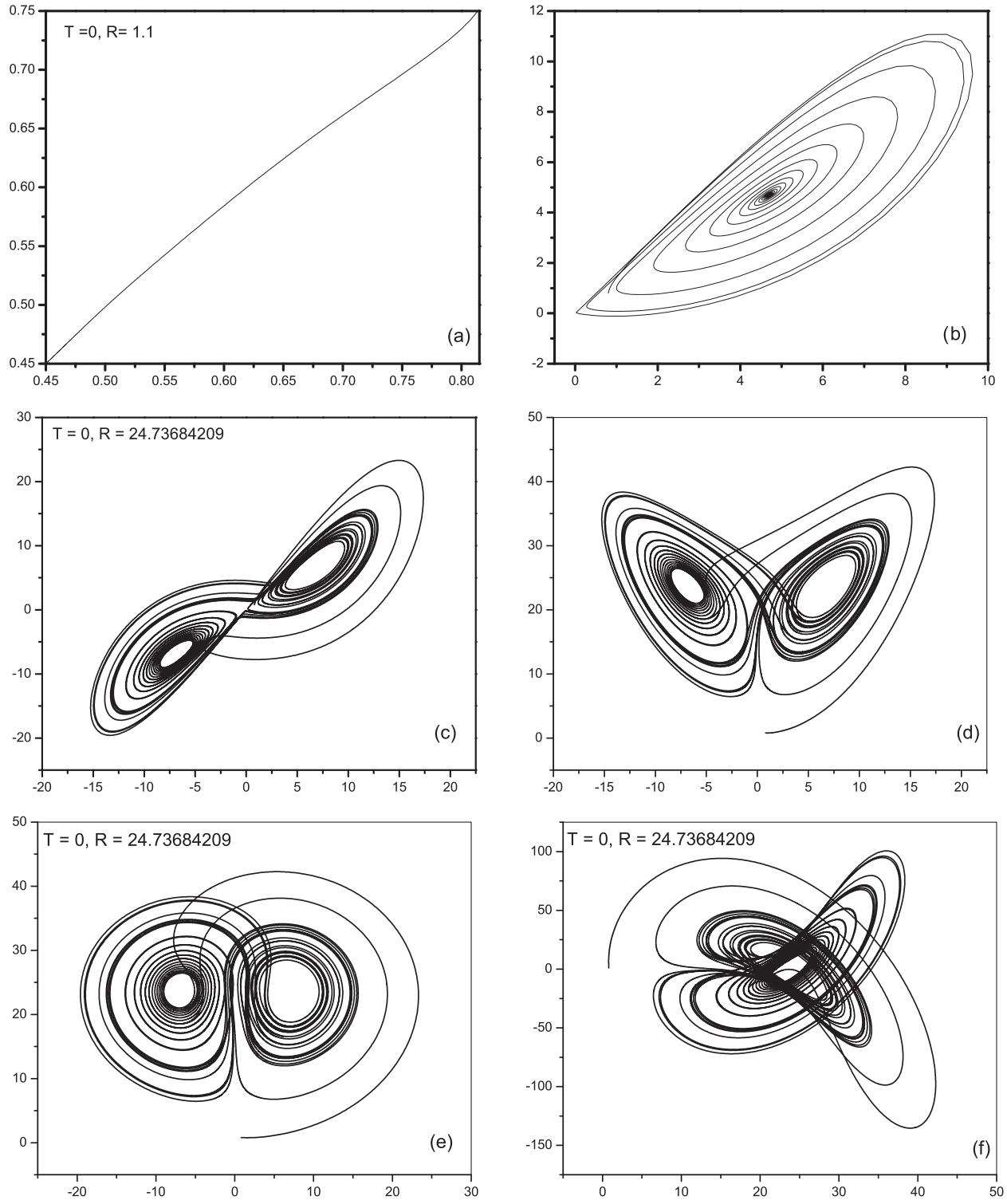

Fig. 3 Phase portraits for evolution of trajectories over time in the state space for increasing value of rescaled Rayleigh number (R). The graphs represent the projection of the solution data points onto $Y-X, Z-X, Z-Y, W-Z$ planes for $\sigma = 10, \gamma = -8/3$ and $T = 0$.

Eq. (35) yields four eigenvalues, and all the roots are real and negative at slightly supercritical value of R, such that the convection fixed points are stable, that is simple nodes. These roots move on the real axis towards the origin as the value of R increases. For $\sigma = 10$ and $\gamma = -8/3$, these roots become equal when $R =$

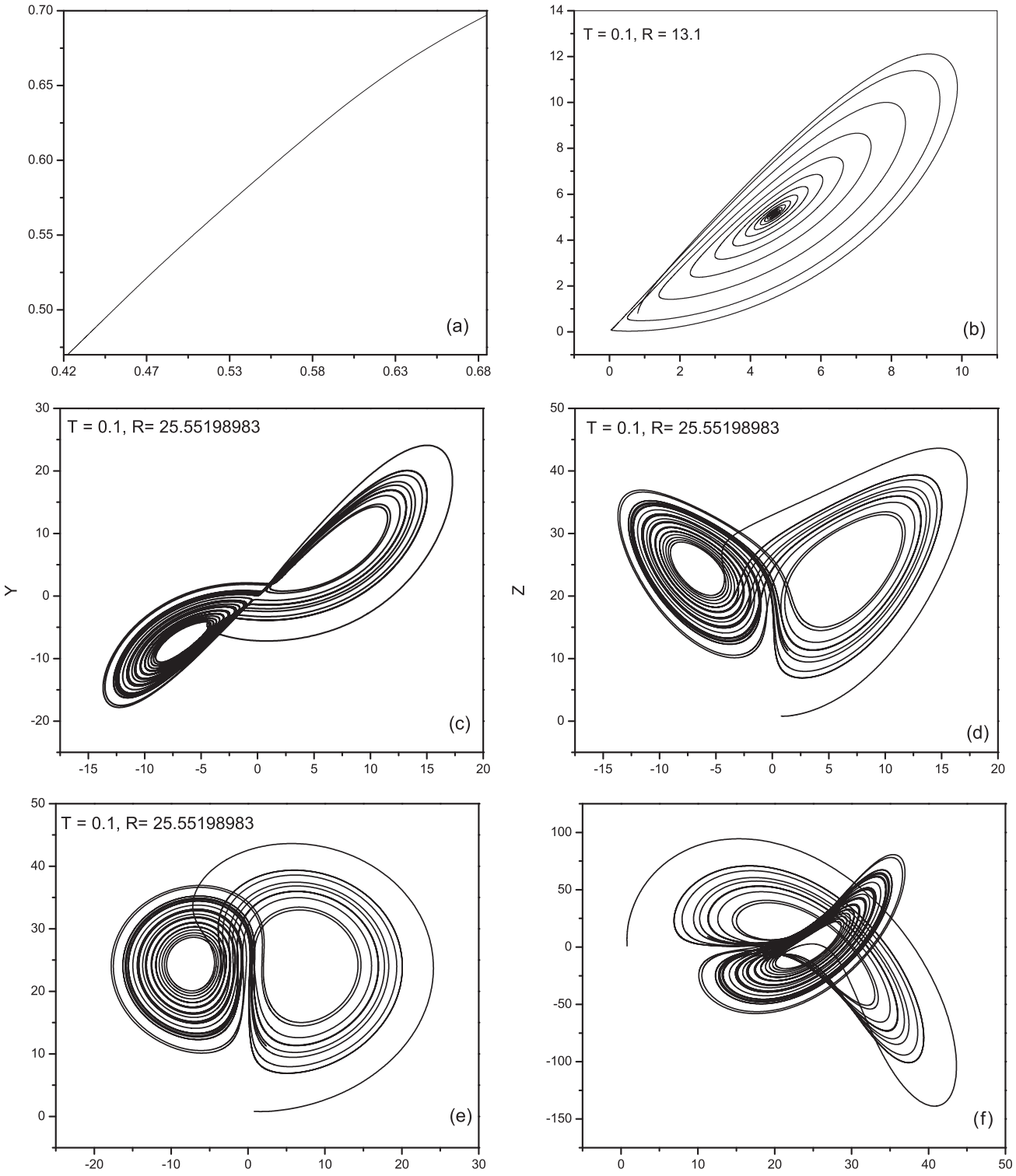

Fig. 4 Phase portraits for evolution of trajectories over time in the state space for increasing value of rescaled Rayleigh number (R). The graphs represent the projection of the solution data points onto $Y-X, Z-X, Z-Y, W-Z$ planes for $\sigma = 10, \gamma = -8/3$ and $T = 0.1$.

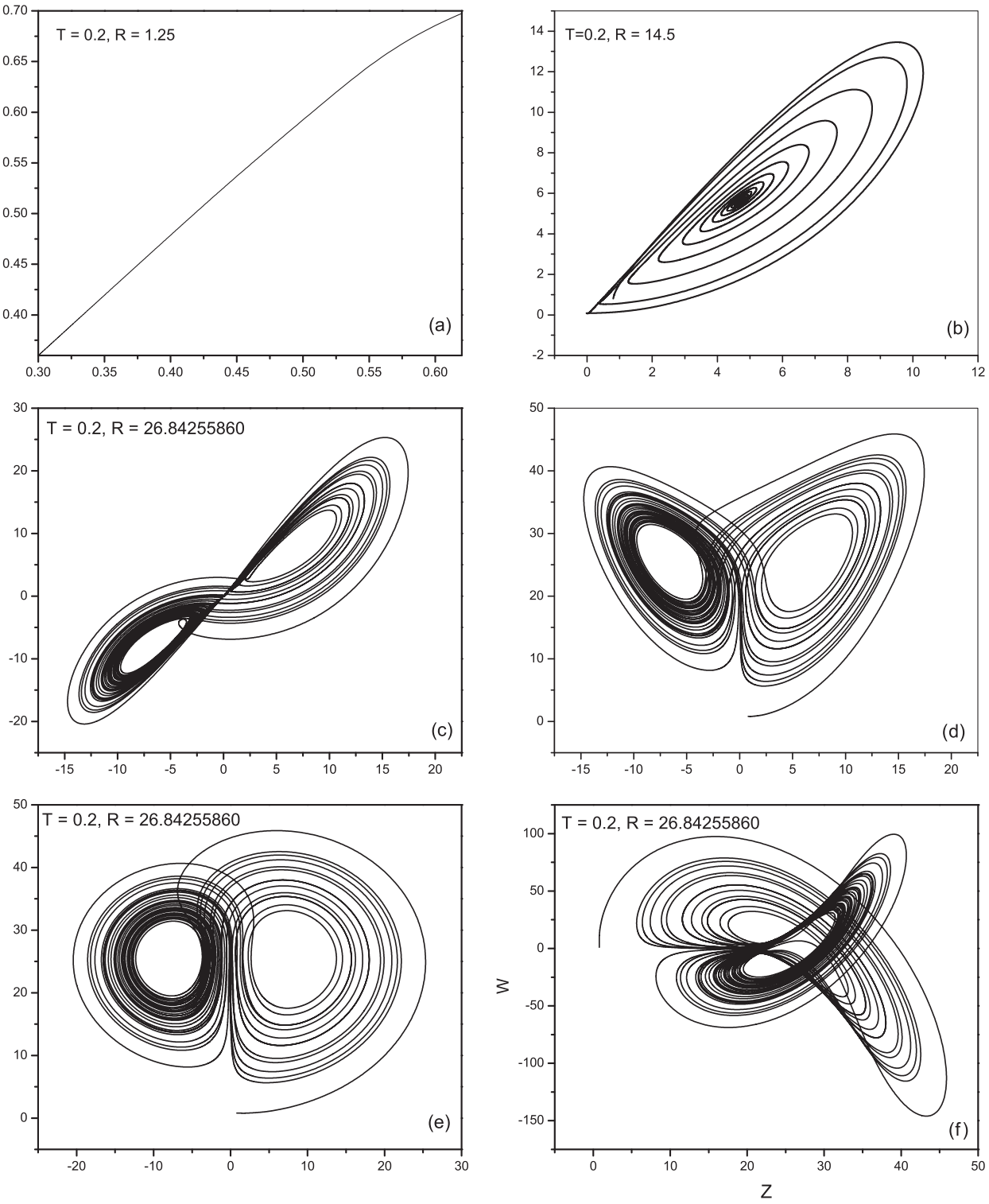

Fig. 5 Phase portraits for evolution of trajectories over time in the state space for increasing value of rescaled Rayleigh number (R). The graphs represent the projection of the solution data points onto $Y-X, Z-X, Z-Y, W-Z$ planes for $\sigma = 10, \gamma = -8/3$ and $T = 0.2$.

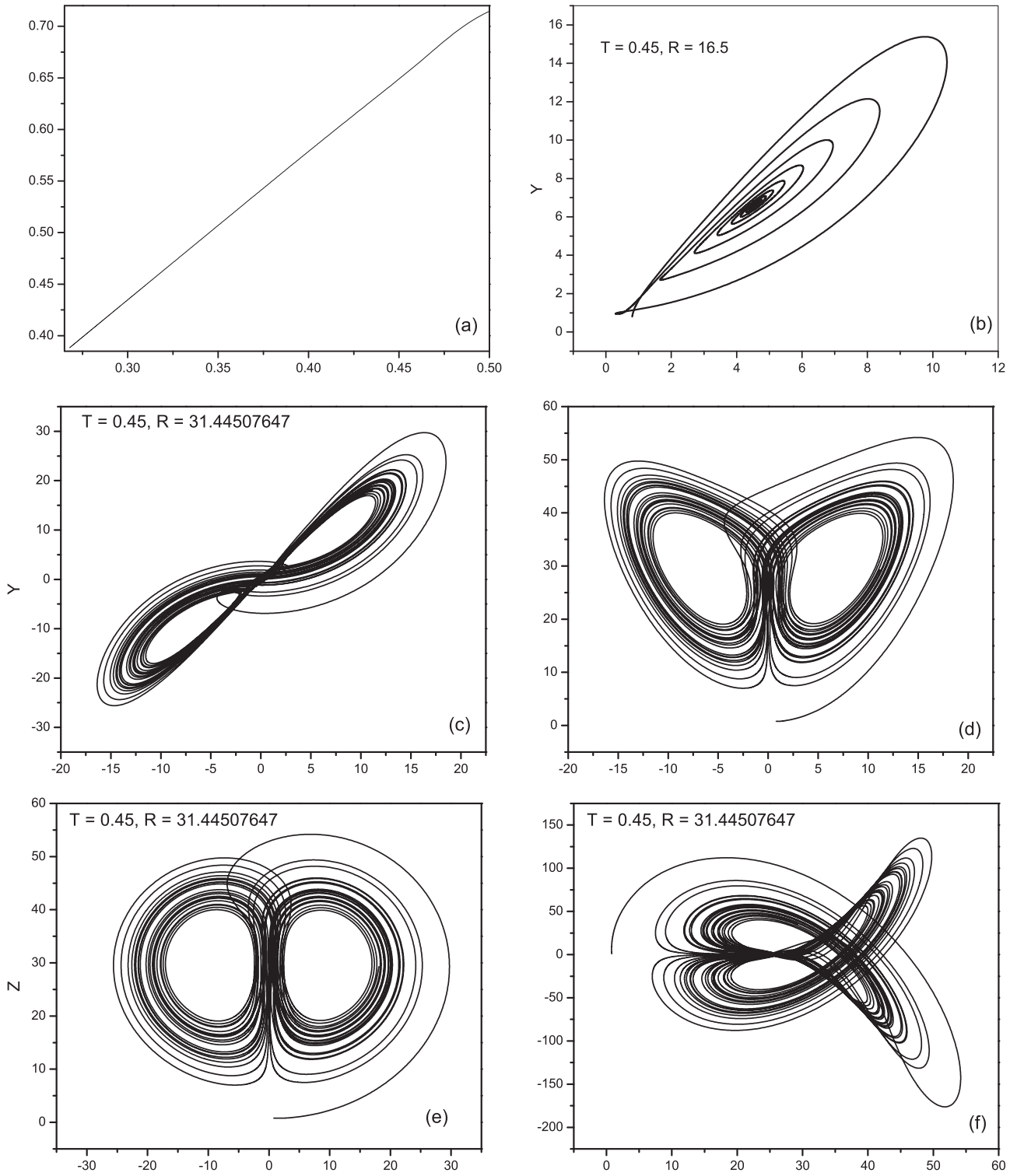

Fig. 6 Phase portraits for evolution of trajectories over time in the state space for increasing value of rescaled Rayleigh number (R). The graphs represent the projection of the solution data points onto $Y-X, Z-X, Z-Y, W-Z$ planes for $\sigma = 10, \gamma = -8/3$ and $T = 0.45$.

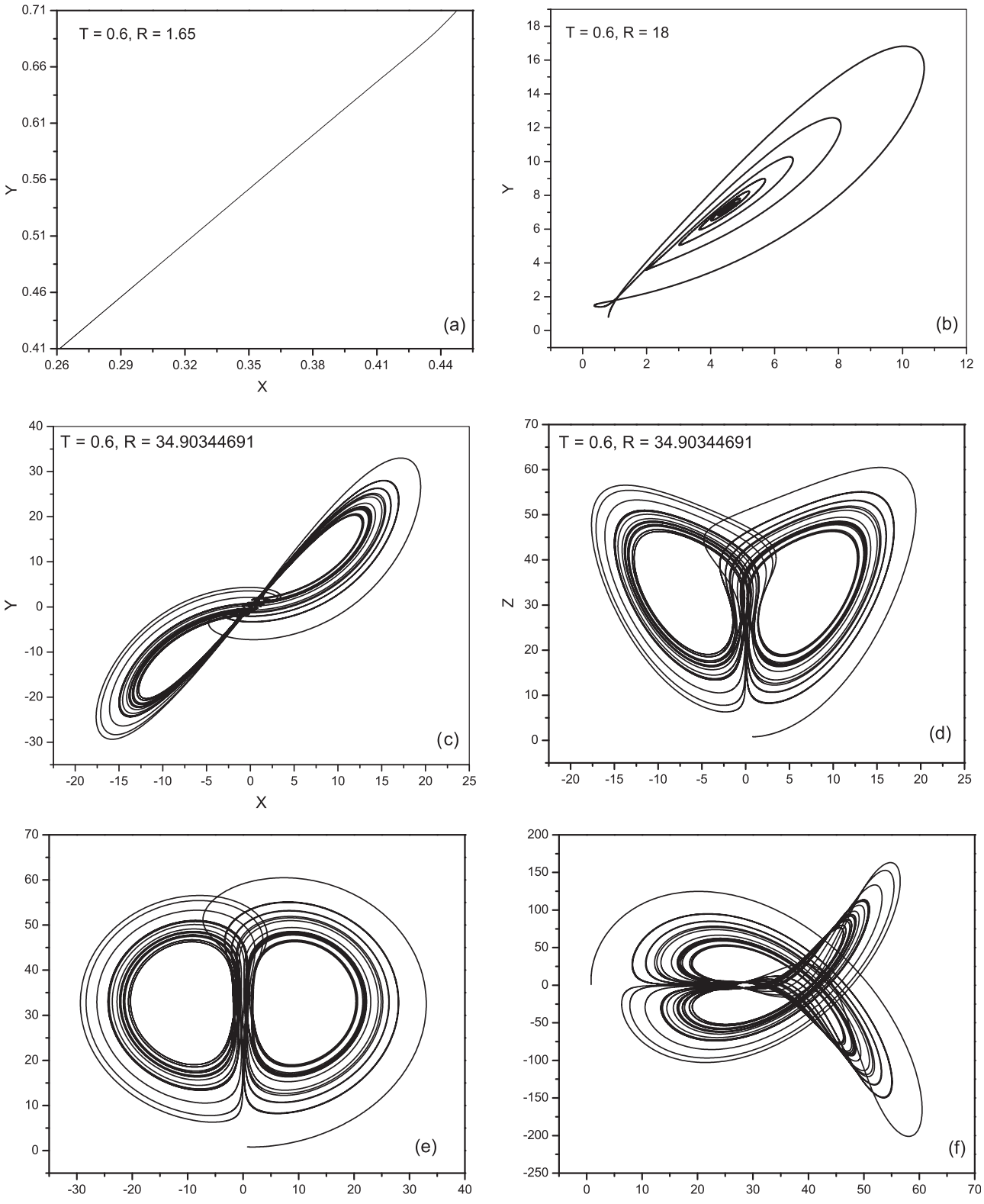

Fig. 7 Phase portraits for evolution of trajectories over time in the state space for increasing value of rescaled Rayleigh number (R). The graphs represent the projection of the solution data points onto $Y-X, Z-X, Z-Y, W-Z$ planes for $\sigma = 10, \gamma = -8/3$ and $T = 0.6$.

$$\frac{\sigma\gamma^2(T+3)(1-\gamma-\sigma-\sigma T)}{(T+1)^2}R^2 - \sigma\gamma\left[(2\sigma+1-\gamma)\left\{\gamma(2-\sigma)+\frac{2\sigma(1-\gamma)(T+3)}{(T+1)} + \sigma(T+3)(\sigma-1)-2\sigma(2\sigma+1-\gamma)\right\}-2\sigma\gamma(T+3)(2-\sigma)\right]R + \sigma^2\gamma(T+1)(2-\sigma)[(2\sigma+1-\gamma)\{2(1-\gamma)+(1-\sigma)(T+1)\} - \gamma(T+1)(2-\sigma)] = 0 \quad (36)$$

At this point the convection fixed points lose their stability and other (periodic or chaotic) solutions take over. The loss of stability of the convection fixed points for $\sigma = 10, \gamma = -8/3$ using Eq. (35) is evaluated to be $R_{c2} = 25.75590$ for $T = 0$, $R_{c2} = 25.343620$ for $T = 0.1$, $R_{c2} = 25.774560$ for $T = 0.2$, $R_{c2} = 29.344020$ for $T = 0.45$ and $R_{c2} = 32.775550$ for $T = 0.6$.

5. Result and discussion

In this section, we present some numerical simulation of the system of Eqs. (23)–(26) for the time domain $0 \leqslant t \leqslant 40$. Calculations were done using Fortran 77 fourth-order Runge–Kutta method on double precision with step size 0.001 and Mathematica, fixing the values $\sigma = 10, \gamma = -8/3$, and taking the initial conditions $X(0) = Y(0) = 0.8, Z(0) = 0.9$ (see Figs. 1 and 2).

In case for $T = 0$, we found that at $R_{c1} = 1$, obtained from Eq. (34), the motionless solution loses stability and the convection solution occurs. Also the eigenvalues from Eq. (35) become equal and complex conjugate when $R = 24.73684209$ (as obtained in Table 1). The convection fixed points lose their stability and a chaotic solution occurs when $R = 24.73684209$. The evolution of trajectories over time in the state space for increasing value of scaled Rayleigh number is shown in Fig. 3 in terms of projections of trajectories onto $Y-X, Z-X, Z-Y$ and $W-Z$ planes. In Fig. 3(a), we observe that the trajectory moves to the steady convection points $X = Y = \sqrt{\frac{\gamma(T+1-R)}{T+1}}$, $Z = -(T+1-R)$ on a straight line for a Rayleigh number slightly above the loss of stability of the motionless solution ($R = 1.1$). At $R = 12$ the trajectories approach the fixed point on a spiral as shown in Fig. 3(b). At the subcritical value of $R = 25.75590$ transition to chaotic behavior solution occurs.

For $T = 0.1$, we obtain $R_{c1} = 1.1$ from Eq. (34), the motionless solution loses stability and convection solution takes over. Moreover, the values of the eigenvalues λ_2 and λ_3 become equal and complex conjugate when $R = 25.55198983$ (shown in Table 1). At the point $R = 25.55198983$ the convection points lose their stability and a chaotic solution occurs. The evolution of trajectories over time in the state space for increasing value of scaled Rayleigh number is presented in Fig. 4 in terms of projections of trajectories onto the $Y-X, Z-X, Z-Y$ and $W-Z$ planes. We observe that in Fig. 4(a), the trajectory moves to the steady convection point $X = Y = \sqrt{\frac{\gamma(T+1-R)}{T+1}}$ and $Z = -(T+1-R)$ on a straight line for a Rayleigh number slightly above the loss of stability of the motionless solution ($R = 1.1$). The trajectories approach a fixed point on a spiral as shown in Fig. 4(b) at $R = 13.1$. At the subcritical value of $R = 25.55198983$ transition to chaotic behavior solution occurs.

For $T = 0.2$, we obtain $R_{c1} = 1.2$ from Eq. (34), the motionless solution loses stability and convection solution takes over. Moreover, the values of the eigenvalues λ_2 and λ_3 become equal and complex conjugate when $R = 26.84255860$ (from Table 1). At the point $R = 26.84255860$ the convection points lose their stability and a chaotic solution occurs. The evolution of trajectories over time in the state space for increasing value of scaled Rayleigh number is presented in Fig. 5 in terms of projections of trajectories onto the $Y-X, Z-X, Z-Y$ and $W-Z$ planes. We observe that in Fig. 5(a), the trajectory moves to the steady convection point $X = Y = \sqrt{\frac{\gamma(T+1-R)}{T+1}}$ and $Z = -(T+1-R)$ on a straight line for a Rayleigh number slightly above the loss of stability of the motionless solution ($R = 1.2$). The trajectories approach a fixed point on a spiral as shown in Fig. 5(b) at $R = 14.5$. At the subcritical value of $R = 26.84255860$ transition to chaotic behavior solution occurs.

For $T = 0.45$, we obtain $R_{c1} = 1.45$ from Eq. (34), the motionless solution loses stability and convection solution takes over. Moreover, the values of the eigenvalues λ_2 and λ_3 become equal and complex conjugate when $R = 31.44507647$. At the point $R = 31.44507647$ the convection points lose their stability and a chaotic solution occurs. The evolution of trajectories over time in the state space for increasing value of scaled Rayleigh number is presented in Fig. 6 in terms of projections of trajectories onto the $Y-X, Z-X, Z-Y$ and $W-Z$ planes. We observe that in Fig. 6(a), the trajectory moves to the steady convection point $X = Y = \sqrt{\frac{\gamma(T+1-R)}{T+1}}$ and $Z = -(T+1-R)$ on a straight line for a Rayleigh number slightly above the loss of stability of the motionless solution ($R = 1.45$). The trajectories approach a fixed point on a spiral as shown in Fig. 6(b) at $R = 16.5$. At the subcritical value of $R = 31.44507647$ transition to chaotic behavior solution occurs.

For $T = 0.6$, we obtain $R_{c1} = 1.6$ from Eq. (34), the motionless solution loses stability and convection solution takes over. Moreover, the values of the eigenvalues λ_2 and λ_3 become equal and complex conjugate when $R = 34.90344691$. At the point $R = 34.90344691$ the convection points lose their stability and a chaotic solution occurs. The evolution of trajectories over time in the state space for increasing value of scaled Rayleigh number is presented in Fig. 7 in terms of projections of trajectories onto the $Y-X, Z-X, Z-Y$ and $W-Z$ planes. We observe that in Fig. 7(a), the trajectory moves to the steady convection point $X = Y = \sqrt{\frac{\gamma(T+1-R)}{T+1}}$ and $Z = -(T+1-R)$ on a straight line for a Rayleigh number slightly above the loss of stability of the motionless solution ($R = 1.6$). The trajectories approach a fixed point on a spiral as shown in Fig. 7(b) at $R = 18$. At the subcritical value of $R = 34.90344691$ transition to chaotic behavior solution occurs.

6. Conclusion

In this paper, we have studied chaotic behavior under the effect of different values of scaled Taylor number T, in a rotating fluid layer, subjected to gravity and heated from below. We found that there is proportional relation between the scaled Taylor number T and scaled Rayleigh number R. This means that chaotic behavior can be delayed (for increasing value of

R) when we increase the scaled Taylor number. We conclude that the transition from steady convection to chaos depends on the level of Taylor number.

References

[1] M.N. Mahmud, I. Hasim, Effect of magnetic field on chaotic convection in fluid layer heated from below, Int. Commun. Heat Mass Trans. 38 (2011) 481–486.

[2] J.M. Jawdat, I. Hashim, Low Prandtl number chaotic convection in porous media with uniform internal heat generation, Int. Commun. Heat Mass Trans. 37 (2010) 629–636.

[3] Carlo Ferrarioa, Arianna Passerinib, Gudrun Thäter, Generalization of the Lorenz model to the two-dimensional convection of second-grade fluids, Int. J. Non-Linear Mech. 39 (2004) 581–591.

[4] Long-Jye Sheu, An autonomous system for chaotic convection in a porous medium using a thermal non-equilibrium model, Chaos Solit. Fractals 30 (2006) 672–689.

[5] L.J. Sheu, L.M. Tam, J.H. Chen, H.K. Chen, K.T. Lin, Y. Kang, Chaotic convection of viscoelastic fluids in porous media, Chaos Solit. Fractals 37 (2008) 113–124.

[6] B.S. Bhadauria, Fluid convection in a rotating porous layer under modulated temperature on the boundaries, Transp. Porous Med. 67 (2007) 297–315.

[7] M.S. Malashetty, Mahantesh Swamy, The effect of rotation on the onset of convection in a horizontal anisotropic porous layer, Int. J. Therm. Sci. 46 (2007) 1023–1032.

[8] M.S. Malashetty, Rajashekhar Heera, The effect of rotation on the onset of double diffusive convection in a horizontal anisotropic porous layer, Transp. Porous Med. 74 (2008) 105–127.

[9] D. Roy, Z.E. Musielak, Generalized Lorenz models and their routes to chaos. II. Energy-conserving horizontal mode truncations, Chaos Solit. Fractals 31 (2007) 747–756.

[10] Eugen Magyari, The butterfly effect in a porous slab, Transp. Porous Med. 84 (2010) 711–715.

[11] P. Vadasz, S. Olek, Weak turbulence and chaos for low Prandtl number gravity driven convection in porous media, Transp. Porous Med. 37 (1999) 69–91.

[12] P. Vadasz, S. Olek, Transition and chaos for free convection in a rotating porous layer, Int. J. Heat Mass Transf. 41 (1999) 1417–1435.

[13] E.N. Lorenz, Deterministic non-periodic flow, J. Atmos. Sci. 20 (1963) 130–142.

[14] C. Sparrow, The Lorenz Equations: Bifurcations, Chaos, and Strange Attractors, Springer-Verlag, New York, 1982.

[15] P. Vadasz, Local and global transitions to chaos and hysteresis in a porous layer heated from below, Transp. Porous Med. 37 (1999) 213–245.

[16] P. Vadasz, Subcritical transitions to chaos and hysteresis in a fluid layer heated from below, Int. J. Heat Mass Transf. 43 (2000) 705–724.

[17] P. Vadasz, S. Olek, Route to chaos for moderate Prandtl number convection in a porous layer heated from below, Transp. Porous Med. 41 (2000) 211–239.

[18] M.N. Mahmud, I. Hasim, Small and moderate Prandtl number chaotic convection in porous media in the presence of feedback control, Transp. Porous Med. 84 (2010) 421–440.

[19] Gupta, K. Vinod, A.K. Singh, A study of Chaos in an anisotropic porous cavity, Int. J. Energy Technol. 5 (27) (2013) 1–12.

[20] Vinod K. Gupta, B.S. Bhadauria, Double diffusive convection in a couple stress fluid saturated sparsely packed porous layer with soret effect using thermal non-equilibrium model. In: Int. Conference on Modeling and Simulation of diffusive Process and Applications, 2012, pp. 89–95.

[21] Vinod K. Gupta, Rajendra Prasad, A.K. Singh, Effect of magnetic field on chaos in couple stress liquid saturated in porous layer, Int. J. Energy Technol. 5 (28) (2013) 1–9.

[22] Vinod K. Gupta, A.K. Singh, Double diffusive reaction convection in viscous fluid layer, Int. J. Ind. Math. 6 (4) (2014) 275–284.